Journal of Applied Mechanics and Technical Physics, Vol. 50, No. 2, pp. 251–260, 2009

MODELING OF SUPERSONIC FLOWS NEAR FLYING VEHICLE ELEMENTS

V. M. Kovenya and A. Yu. Slyunyaev

UDC 533.6

Supersonic flows near flying vehicle elements are calculated in the approximation of the full Navier–Stokes equations for a viscous compressible heat-conducting gas with different values of free-stream Mach and Reynolds numbers and angles of attack. The main laws of the flow near the lifting surface and in the inlet are obtained.

Key words: *Navier–Stokes equations, difference scheme, supersonic flow, separation, shock waves.*

Introduction. The interest in flying vehicles capable of reaching hypersonic velocities has been recently revived. Testing of full-scale models in hypersonic wind tunnels incurs significant financial expenses owing to the necessity of conducting extensive research on choosing the vehicle configuration and identifying the specific features of the gas flow in various flight regimes. At the same time, the current level of development of mathematical modeling allows full mathematical models, which describe the flow near the vehicle surface in a wide range of flow parameters, to be used to solve this class of problems. As a consequence, real physical processes can be modeled with sufficient accuracy. Thus, financial and time expenses necessary to design modern flying vehicles can be substantially reduced.

The most full mathematical model that describes the physical processes proceeding near the surface of flying vehicles or their elements is the model that involves the Navier–Stokes equations for a compressible heat-conducting gas. Solutions of the Navier–Stokes equations are usually characterized by the presence of subdomains with large gradients and other specific features, such as boundary layers, barrel shock waves, separation regions, etc., which imposes rigorous constraints on numerical algorithms used. These algorithms should be conservative and efficient; they have to possess necessary accuracy and sufficient stability for the problem solution to be obtained on available computers within reasonable time. The most popular algorithms are reviewed in [1–6].

The present paper describes the results of modeling of supersonic and hypersonic flows near flying vehicle elements within the framework of the full Navier–Stokes equations for a compressible heat-conducting gas. The solution of the Navier–Stokes equations is found by the scheme of approximate factorization with special splitting of operators [7, 8]. A steady supersonic viscous gas flow in the plane of symmetry of the model vehicle described in [9] is studied numerically. The problem solution is sought in the flow near the lifting surface of the vehicle, including the flow in the inlet duct simulating the scramjet duct and in the near wake. The study is performed for different free-stream Mach and Reynolds numbers and for different angles of attack of the vehicle.

1. Formulation of the Problem and Numerical Algorithm. The flow around a vehicle whose elements are shown in Fig. 1 was studied numerically within the framework of the full Navier–Stokes equations for a compressible heat-conducting gas. For convenience of integration and analysis of results, the initial Navier–Stokes equations were brought to dimensionless form. The dimensionless parameters were chosen to be the characteristic length of the vehicle L, gas density ρ_0, free-stream velocity u_0, and free-stream temperature T_0. The vehicle was assumed to be plane and to have a blunted leading edge; the upper generatrix had three points of inflection upstream of the inlet-duct entrance: $x = 3.0$, 3.8, and 4.5. The first segment of the generatrix (up to the first inflection point) was defined by the expression $1 - 0.057\sqrt{x}$, and the remaining segments were defined by a piecewise-linear function

Institute of Computational Technologies, Siberian Division, Russian Academy of Sciences, Novosibirsk 630090; kovenya@ict.nsc.ru. Translated from Prikladnaya Mekhanika i Tekhnicheskaya Fizika, Vol. 50, No. 2, pp. 98–108, March–April, 2009. Original article submitted September 29, 2008.

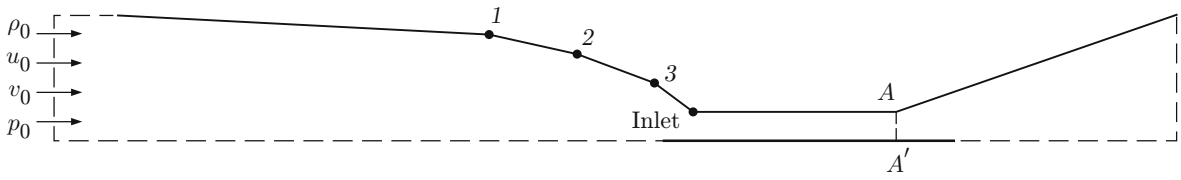

Fig. 1. Computational domain: the points of the first, second, and third inflections of the surface are indicated by 1, 2, and 3, respectively.

(see Fig. 1). The angle of inclination of the second segment of the generatrix (between the first and second inflection points) was $15°49'$, the angle of inclination of the third segment was $16°$, and the angle of inclination of the fourth segment was $24°$. A similar geometric configuration was used in [9]. The characteristic length L was chosen to be the distance between the lower plane of the inlet and the tip of the vehicle. The inlet-duct height was $0.25L$. The study was performed for two configurations of the computational domain: in the first case, the computational domain was bounded by the line AA' (see Fig. 1); in the second case, the calculations were performed in the entire computational domain containing the region of flow exhaustion from the duct with the solid upper boundary.

The following boundary conditions were imposed in numerical simulations: an unperturbed supersonic flow with the parameters $\rho\Big|_\Gamma = 1.0$ and $p\Big|_\Gamma = 1/(\gamma \mathrm{M}^2)$ was set on the input boundary; the components of the velocity vector were defined by the expressions $u\Big|_\Gamma = \cos\alpha$ and $v\Big|_\Gamma = \sin\alpha$, where α is the angle of attack of the incoming flow. Conditions of thermal insulation $(\partial T/\partial n)\Big|_\Gamma = 0$ or the temperature $T_1 = 4T_0$ and no-slip conditions for velocity $u\Big|_\Gamma = v\Big|_\Gamma = 0$ were imposed on the vehicle surface (solid curves in Fig. 1). The flow at the duct exit was subjected to soft boundary conditions $(\partial^2 \boldsymbol{f}/\partial x^2)\Big|_\Gamma = 0$, where $\boldsymbol{f} = (\rho, u, v, T)^{\mathrm{t}}$. The dimensionless dynamic viscosity μ and thermal conductivity κ were defined as power-law functions of temperature with a power index $\omega = 0.76$, the second viscosity μ' was assumed to be equal to zero, the ratio of specific heats was $\gamma = 1.4$, and the Prandtl number was $\mathrm{Pr} = 0.72$. With allowance for the chosen dimensionless parameters, the flow was defined by the free-stream Mach and Reynolds numbers and by the angle of attack α. The steady solution of the problem was found by a time-dependent method. The values of unperturbed velocity, density, and temperature at the input cross section were used as the initial distributions.

The method used to solve the problem in the present paper was a combined method of splitting in terms of physical processes and spatial variables, which was proposed in [7, 8]. Implementation of the algorithm in the form of an implicit difference scheme realized on fractional steps by scalar sweeps allowed us to eliminate rigorous constraints on grid steps typical of explicit schemes. The proposed scheme is conservative; thus, it can be used to solve steady and unsteady problems. The scheme was described in detail in [7].

Let us consider the Navier–Stokes equations in Cartesian coordinates in divergent form (see, e.g., [10]). In the computational domain (see Fig. 1) where the numerical solution is sought, we apply a nondegenerate transformation of coordinates $q_j = q_j(x_i)$, $j = 1, 2$, which transforms this domain to a unit square. We also assume that there exists an inverse nondegenerate transformation of coordinates $x_j = x_j(q_i)$. Then, the system of the Navier–Stokes equations can be written in conservative form in the new variables as well (see [8]):

$$\frac{\partial \boldsymbol{U}}{\partial t} = \boldsymbol{W}, \qquad \boldsymbol{W} = -\sum_{j=1}^{N} \frac{\partial \boldsymbol{W}_j}{\partial q_j}. \tag{1}$$

Here

$$\boldsymbol{U} = \frac{1}{J}\begin{pmatrix} \rho \\ \rho v_1 \\ \rho v_2 \\ E \end{pmatrix}, \qquad \boldsymbol{W}_j = \frac{1}{J}\begin{pmatrix} \rho U_j \\ \rho v_1 U_j + q_j^1 p - G_j^1 \\ \rho v_2 U_j + q_j^2 p - G_j^2 \\ (E+p)U_j + Q_j - R_j \end{pmatrix},$$

$$J = \det \begin{pmatrix} q_1^1 & q_1^2 \\ q_2^1 & q_2^1 \end{pmatrix} = q_1^1 q_2^1 - q_1^2 q_2^1$$

is the coordinate transformation Jacobian,

$$q_j^i = \frac{\partial q_i}{\partial x_j}, \quad U_j = \sum_{i=1}^{2} q_j^i v_i, \quad G_j^l = \sum_{m=1}^{2} q_m^j \sigma_l^m, \quad R_j = \kappa \sum_{l=1}^{2} q_j^l \frac{\partial T}{\partial q_l}, \quad Q_j = \sum_{m=1}^{1} v_m \sigma_j^m,$$

$$\sigma_j^i = \delta_j^i \lambda \operatorname{div} \boldsymbol{v} + \mu \sum_{l=1}^{2} \Big(q_i^l \frac{\partial v_j}{\partial q_l} + q_j^l \frac{\partial v_i}{\partial q_l} \Big), \qquad \operatorname{div} \boldsymbol{v} = \sum_{j=1}^{2} \sum_{l=1}^{2} q_j^l \frac{\partial v_j}{\partial q_l}.$$

Let us present the Navier–Stokes equations (1) in nondivergent form as

$$\frac{\partial \boldsymbol{f}}{\partial t} + \sum_{j=1}^{2} B_j \boldsymbol{f} = \boldsymbol{F},$$

where

$$\boldsymbol{f} = \begin{pmatrix} \rho \\ v_1 \\ v_2 \\ p \end{pmatrix}, \qquad B_j = \begin{pmatrix} \dfrac{\partial}{\partial q_j} U_j & 0 & 0 & 0 \\ 0 & U_j \dfrac{\partial}{\partial q_j} - G_j^1 & 0 & a_j^1 \dfrac{\partial}{\partial q_j} \\ 0 & 0 & U_j \dfrac{\partial}{\partial q_j} - G_j^2 & a_j^2 \dfrac{\partial}{\partial q_j} \\ 0 & c_j^1 \dfrac{\partial}{\partial q_j} & c_j^2 \dfrac{\partial}{\partial q_j} & U_j \dfrac{\partial}{\partial q_j} - G_j^3 \end{pmatrix},$$

$$a_j^l = \frac{q_j^l}{\rho}, \quad c_j^l = \gamma p q_j^l, \quad G_j^l = \frac{1}{\rho} \sum_{m=1}^{2} q_m^j \frac{\partial}{\partial q_j} b_m^l q_l^j \frac{\partial}{\partial q_j}, \quad G_j^3 = \sum_{m=1}^{2} q_m^j \frac{\partial}{\partial q_j} \kappa_{q_m^j} \frac{\partial}{\partial q_j} \frac{1}{\rho}.$$

The matrix operators B_j include convective terms, terms with pressure, and viscous terms containing only the repeated derivatives in each direction q_j, while the vector $\boldsymbol{F}$ contains the remaining terms of the equations. We approximate the initial operators B_j by the difference operators B_{jh} with the order $O(h^k)$ and introduce splitting of the operators B_{jh} into their sum:

$$B_{jh}^1 = \begin{pmatrix} 0 & 0 & 0 & 0 \\ 0 & 0 & 0 & a_j^1 \overline{\Lambda}_j \\ 0 & 0 & 0 & a_j^2 \overline{\Lambda}_j \\ 0 & c_j^1 \Lambda_j & c_j^2 \Lambda_j & U_j^n \Lambda_j - G_{jh}^3 \end{pmatrix},$$

$$B_{jh}^2 = \begin{pmatrix} \Lambda_j U_j^n & 0 & 0 & 0 \\ 0 & U_j^n \Lambda_j - G_{jh}^1 & 0 & 0 \\ 0 & 0 & U_j \dfrac{\partial}{\partial q_j} - G_{jh}^2 & 0 \\ 0 & 0 & 0 & 0 \end{pmatrix}. \tag{2}$$

For the numerical solution of the system of the Navier–Stokes equations, we use the scheme of approximate factorization (see [7, 8])

$$\prod_{j=1}^{2} (I + \tau \alpha B_{jh}^1)(I + \tau \alpha B_{jh}^2) \frac{\boldsymbol{f}^{n+1} - \boldsymbol{f}^n}{\tau} = -(A_h^{-1})^n \boldsymbol{W}_h^n \tag{3}$$

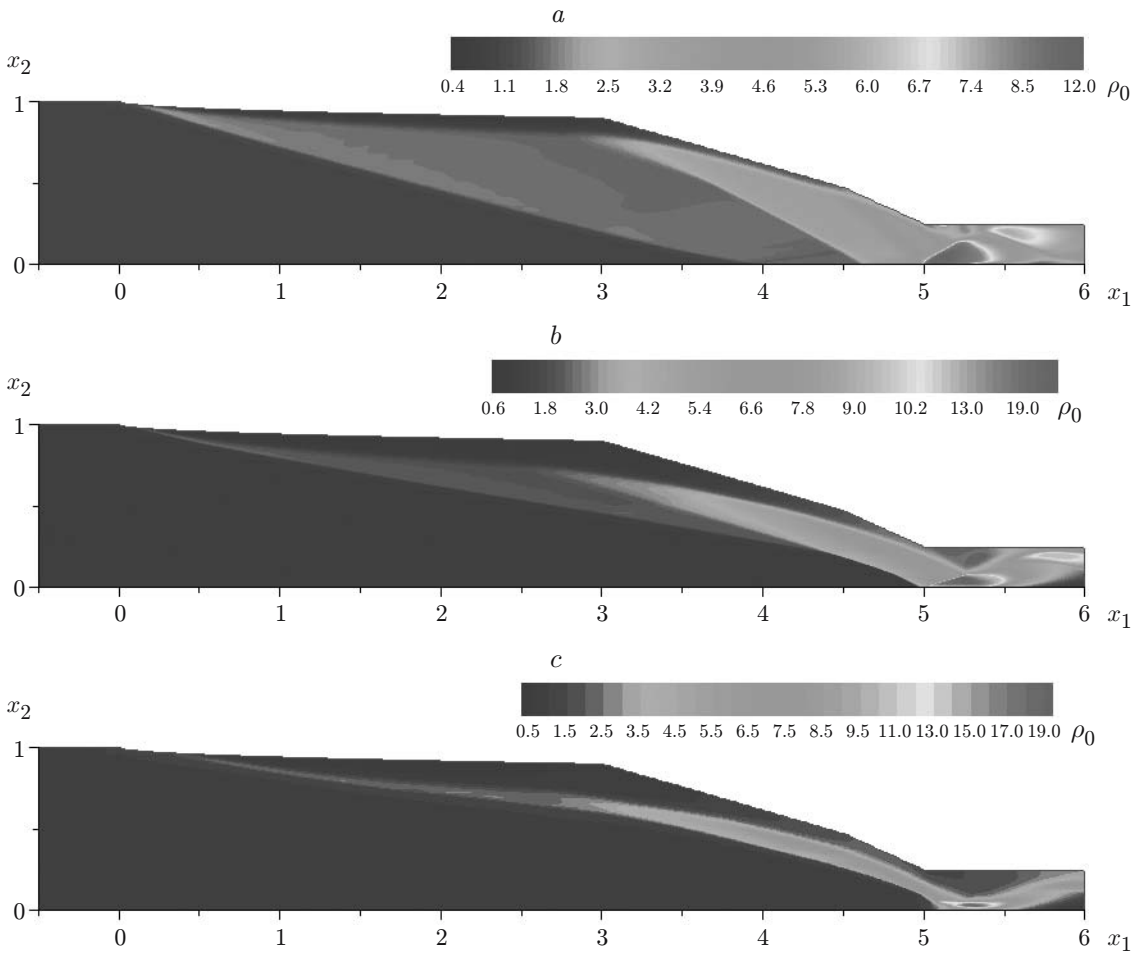

Fig. 2. Distributions of gas density for different Mach numbers: $M_0 = 4$ (a), 6 (b), and 8 (c).

or an equivalent scheme in fractional steps

$$\boldsymbol{\xi}^n = -(A_h^{-1})^n \boldsymbol{W}_h^n, \qquad (I + \tau\alpha B_{1h}^1)\boldsymbol{\xi}^{n+1/4} = \boldsymbol{\xi}^n,$$

$$(I + \tau\alpha B_{1h}^2)\boldsymbol{\xi}^{n+1/2} = \boldsymbol{\xi}^{n+1/4}, \qquad (I + \tau\alpha B_{2h}^1)\boldsymbol{\xi}^{n+3/4} = \boldsymbol{\xi}^{n+1/2}, \tag{4}$$

$$(I + \tau\alpha B_{2h}^2)\boldsymbol{\xi}^{n+1} = \boldsymbol{\xi}^{n+3/4}, \qquad \boldsymbol{f}^{n+1} = \boldsymbol{f}^n + \tau\boldsymbol{\xi}^{n+1}.$$

The difference scheme (3) or (4) approximates the Navier–Stokes equations with the order $O(\tau + h^2)$ for all α and becomes conservative after a steady state is reached. As it follows from the form of the matrix operators B_{jh}^l in (2), implementation of this scheme on fractional steps reduces to three-point scalar sweeps, which makes this algorithm efficient.

2. Results of Numerical Calculations. Using the algorithm described in Sec. 1, we calculated the flow in the central longitudinal section of a flying vehicle consisting of the following elements: lifting surface, inlet duct, and aft part. The majority of the calculations were performed on a difference grid containing 326×161 nodes, with different values of the Mach and Reynolds numbers. The results of test calculations and some results of calculations of the duct flow with gas injection from some part of the duct surface can be found in [8]. Some results for the flow around the vehicle elements for $\mathrm{Re} = 10^4$, $\alpha = 6°$, and $M_0 = 4$, 6, and 8 are described below.

Figure 2 shows the density field for different Mach numbers. As the free-stream velocity increases, the angle of the bow shock wave arising in a supersonic flow decreases with increasing Mach number. The bow shock wave does not enter the duct at all at $M_0 = 4$ (Fig. 2a), is incident onto the lower edge of the inlet at $M_0 = 6$ (Fig. 2b),

and penetrates into the inlet duct at $M_0 = 8$ (Fig. 2c). Shock waves emanate from the points of inflection of the upper generatrix (see, e.g., Fig. 2a) and interact with the bow shock wave. Another bow shock wave appears near the lower edge of the duct and interacts with the incident bow shock wave. The flow density and pressure in the initial cross section of the inlet drastically increase. The shock wave propagating from the lower edge of the duct is incident onto the upper wall of the inlet and leads to flow separation whose intensity depends on the free-stream Mach number. An increase in the Mach number results in a greater size of the reverse flow region formed on the upper wall of the duct.

Figure 3 shows the Mach number distributions in the duct cross section $x = 5.3$. The maximum height of the reverse flow region is observed at $M_0 = 8$, while the width of the supersonic flow region decreases with increasing Mach number. Thus, the width of the supersonic flow region in the duct is 80% of the inlet-duct width at $M_0 = 4$, 48% at $M_0 = 6$, and 38% at $M_0 = 8$.

In the second series of calculations, we studied the effect of the free-stream angle of attack on the flow character in the vicinity of the vehicle. The calculations were performed for angles of attack $\alpha = 0$, 3, 9, and 15° and Mach number $M_0 = 6$. Figure 4 shows the isolines of gas density in the inlet duct. At free-stream angles of attack $\alpha < 9°$ and $\alpha \geqslant 9°$, different flow regimes are observed in the vicinity of the duct entrance. At low angles of attack, the bow shock wave does not enter the duct, whereas a more complicated flow pattern with a triple configuration and a barrel shock is formed ahead of the duct entrance at high angles of attack.

The flow pattern inside the duct is illustrated in more detail in Fig. 5, which shows the vector velocity fields. At high angles of attack, the supersonic gas flow zone becomes substantially narrower and reaches a minimum value at $\alpha = 15°$ (Fig. 5d); a stagnant zone is formed behind the barrel shock wave. At low angles of attack of the incoming flow (Figs. 5a and 5b), an extended reverse flow zone is formed on the upper wall of the duct. The calculations predict that the minimum size of the reverse flow region near the upper surface of the duct is reached at angles of attack $\alpha \geqslant 9°$ (Figs. 5c and 5d).

Figure 6 shows the distributions of the friction coefficient on the upper surface of the body. Small regions of flow separation are formed near the inflection point of the generatrix of the lifting surface and ahead of the duct entrance. Note that there is no separation of the boundary layer on the upper wall of the surface ahead of the inlet entrance at low angles of attack. The velocity of the gas flow passing through the barrel shock decreases to a subsonic velocity and then increases to a supersonic velocity again further downstream.

The third series of calculations modeled the flow for the entire vehicle configuration (lifting surface, inlet duct, and aft part). The calculations were performed for $M_0 = 6$ and $\alpha = 3°$; the computational grid contained 451×161 nodes. In contrast to the geometry used in the second series of calculations, the lower edge of the inlet began at a point $x_1 = 4.7$, and the rear edge of the duct had a coordinate $x_1 = 7$. In this flow regime, the bow shock wave does not enter the inlet duct. The shock wave propagating from the lower edge of the duct is incident onto the upper wall and induces flow separation (Fig. 7). A wide zone of the low-velocity flow is developed on the lifting surface of the vehicle. A separated flow zone arises on the lower wall of the duct in the vicinity of the point $x_1 = 6$, which is caused by shock-wave reflection from the upper wall of the duct.

The calculations predict that a narrow supersonic zone with the gas temperature increasing by a factor of 4 to 8 is formed in the duct. After the flow passes through this zone, the gas velocity increases, and the temperature decreases. The gas velocity in the expanding region behind the duct exit increases and becomes almost equal to the free-stream velocity, while the gas temperature, vice versa, decreases and reaches $T \approx 2T_0$.

The gas temperature on the solid walls of the duct reaches $T \approx 8T_0$ (Fig. 8), which is caused by sudden deceleration of the flow. Further downstream, only a small change in the wall temperature is observed. The presence of such thermal loads on the duct wall necessitates heat removal from the surface; therefore, a constant temperature $T_1 = 4T_0$ was set on the duct walls in the calculations instead of the thermal insulation condition. The calculations were performed for $M_0 = 6$ and $\alpha = 6$ and 12°. A change in the boundary conditions for temperature leads to a significant change in the flow structure. The distributions of the gas density in the computational domain are plotted in Fig. 9. The bow shock wave propagating from the vehicle tip and the shock wave induced at the generatrix inflection point intersect and merge together into one shock wave, which enters the inlet duct. Forced cooling of the walls shifts the zone with the maximum temperature to the region of wave interaction with the wall ($x_1 = 5$).

Maintaining a constant temperature of the duct walls leads to disappearance of gas separation regions on the upper wall of the duct at $\alpha = 6$ and 12° (Fig. 10). After the flow passes over the inlet duct, the velocity recovers

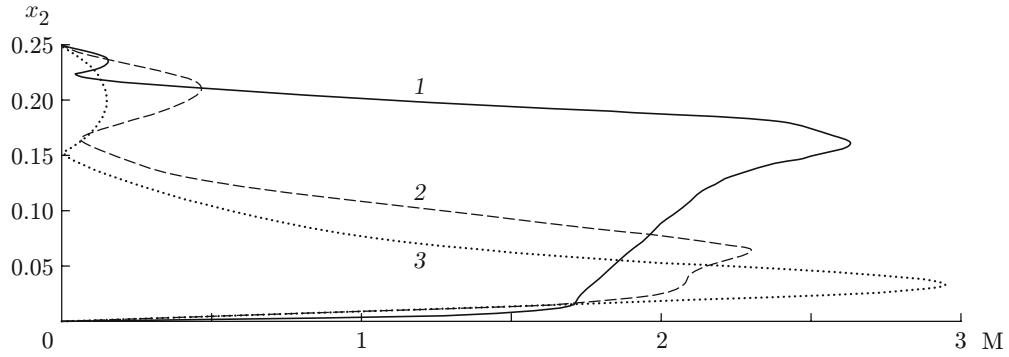

Fig. 3. Distributions of the Mach numbers ($x = 5.3$): $M_0 = 4$ (1), 6 (2), and 8 (3).

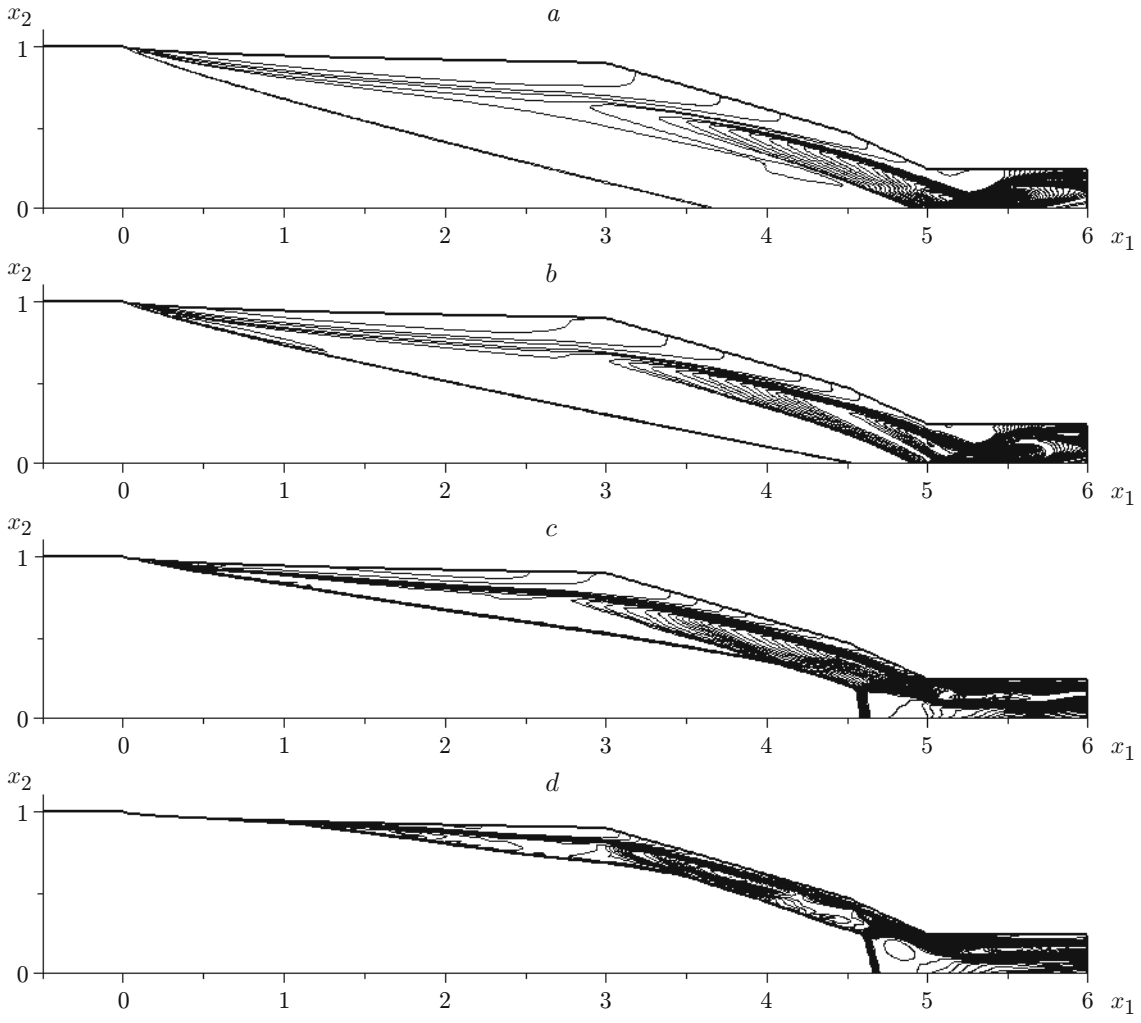

Fig. 4. Gas density isolines for $\alpha = 0^\circ$ (a), 3° (b), 9° (c), and 15° (d).

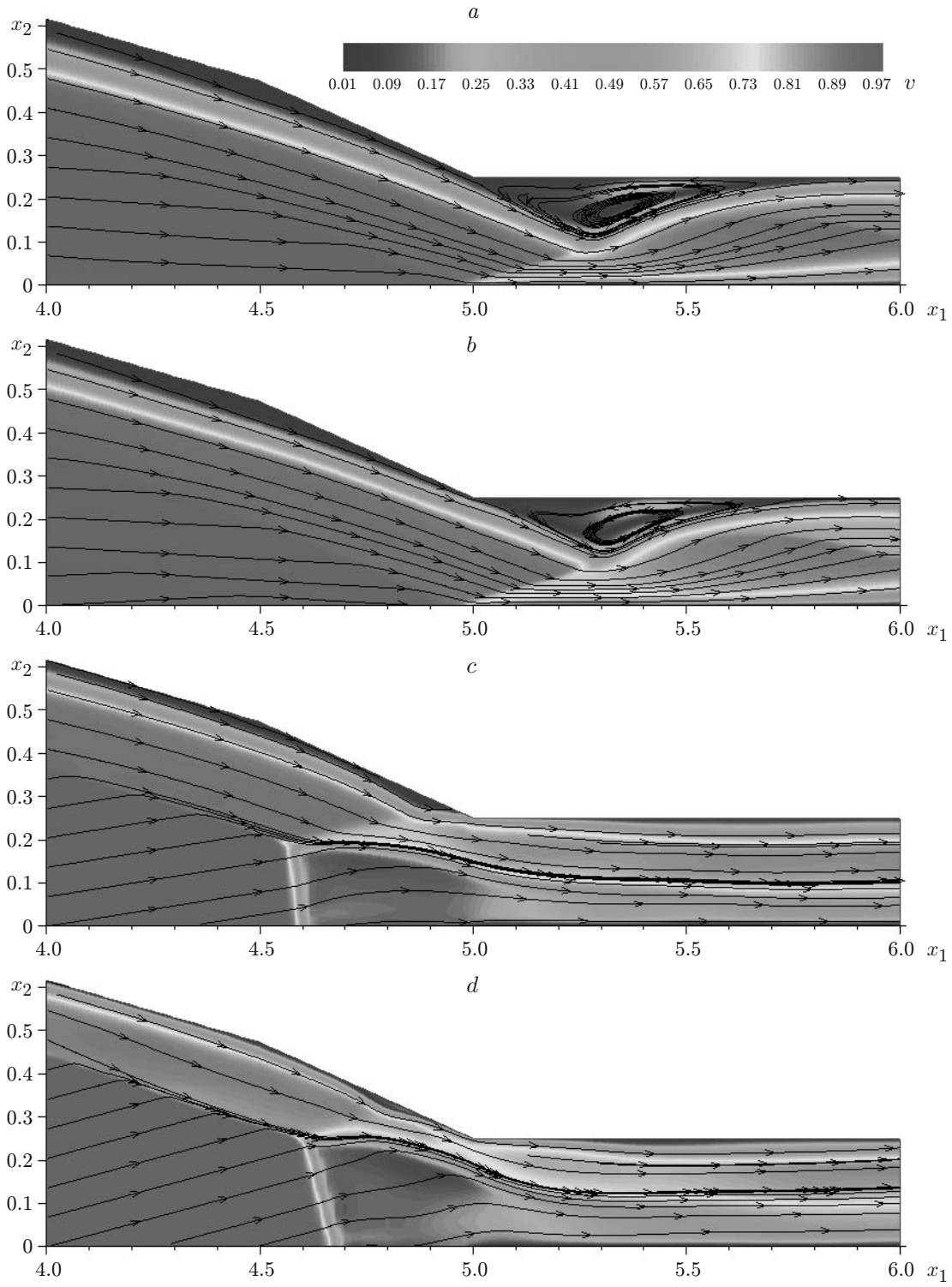

Fig. 5. Velocity field in the domain $x = 4$–6 for $\alpha = 0^\circ$ (a), 3° (b), 9° (c), and 15° (d).

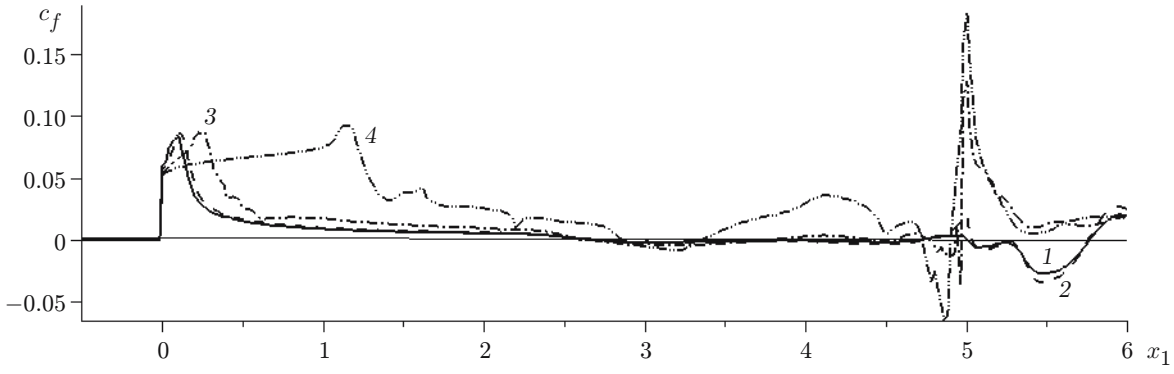

Fig. 6. Distributions of the friction coefficient on the body surface for $\alpha = 0^\circ$ (1), 3° (2), 9° (3), and 15° (4).

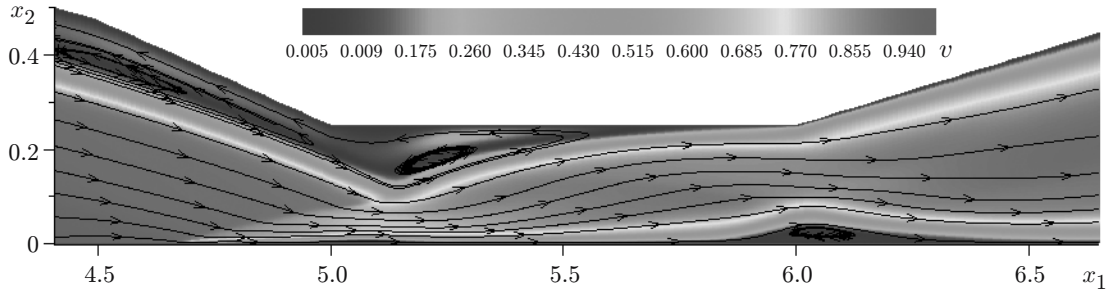

Fig. 7. Velocity field in the duct.

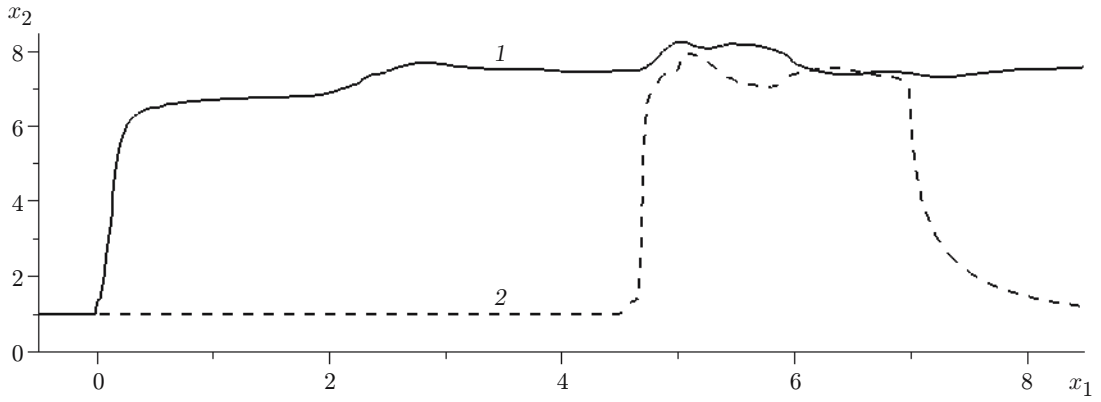

Fig. 8. Distributions of the gas temperature on the upper (1) and lower (2) walls of the duct.

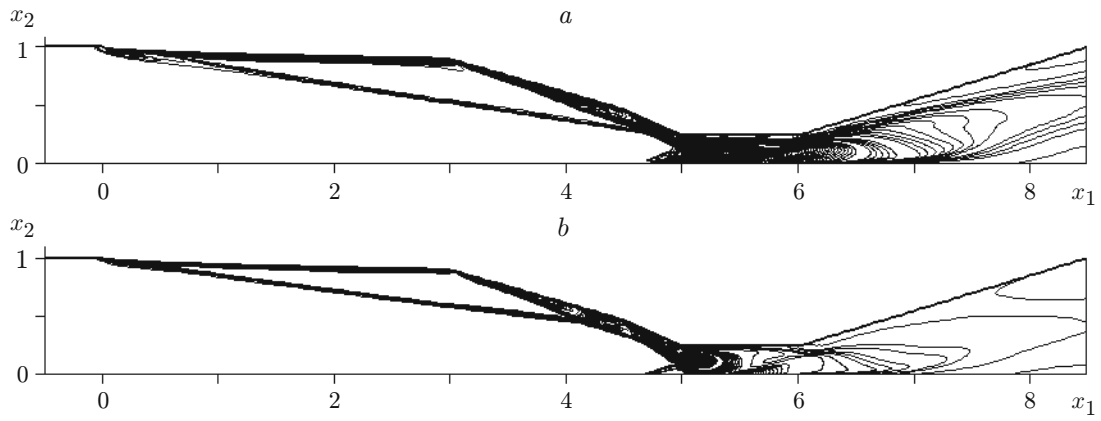

Fig. 9. Gas density isolines: $\alpha = 6^\circ$ (a) and 12° (b).

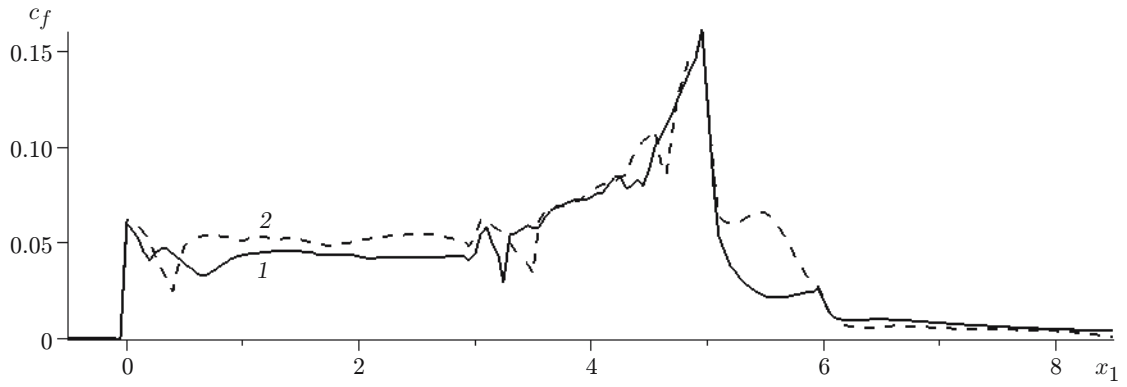

Fig. 10. Distributions of the friction coefficient on the upper wall for $\alpha = 6^\circ$ (1) and 12° (2).

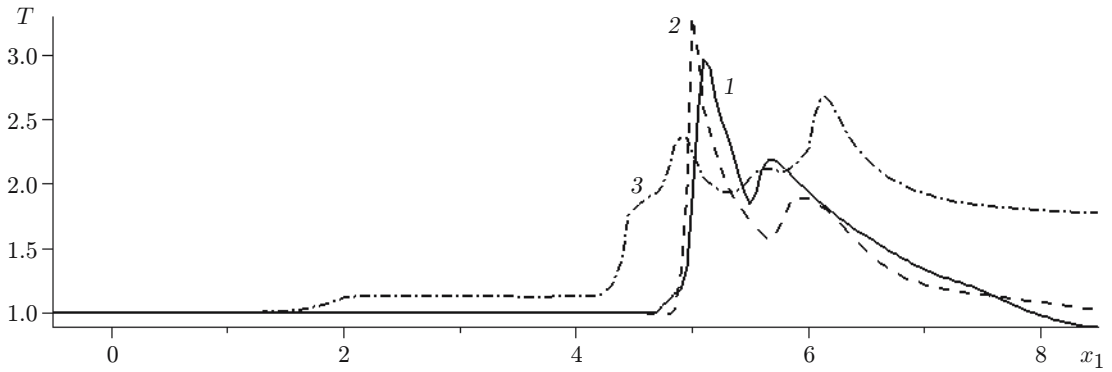

Fig. 11. Temperature distributions in longitudinal sections: $x_2 = 0.25$ (1), 0.50 (2), and 0.75 (3).

its free-stream value. It follows from the calculations that the minimum velocity of the gas in the duct is supersonic and corresponds to M $\approx$ 3. Recall that the flow velocity decreases to subsonic values if the condition of thermal insulation on the duct walls is specified.

An analysis of the distributions of the gas temperature in different longitudinal sections (Fig. 11) shows that the maximum temperature of the gas in the duct decreases owing to cooling of the duct walls. An analysis of results calculated for gas flows in a duct with a specified temperature allows us to conclude that forced cooling of the solid duct walls leads to reduction of thermal loads and, as a consequence, to disappearance of extended separation regions near the duct walls. A change in the vehicle geometry (longer lower wall of the duct) alters the shock-wave structure: a detached shock wave does not arise ahead of the duct, thus, the gas flow rate in the duct increases.

Conclusions. The numerical algorithm used in this work allows a fairly accurate study of supersonic viscous heat-conducting gas flows around various bodies. A numerical study of viscous supersonic flows near vehicle elements was performed for a fixed Reynolds number and varied Mach numbers and angles of attack. The influence of the free-stream parameters on the character of the duct flow was studied, and the main laws of variations of the latter were established. The effect of the vehicle geometry and boundary conditions on the wall on flow characteristics was considered. Obtaining aerodynamic characteristics of flying vehicles of this type requires more extensive computations.

This work was supported by the Russian Foundation for Basic Research (Grant No. 08-01-00264a).

REFERENCES

1. C. Fletcher, *Computational Techniques for Fluid Dynamics*, Springer-Verlag, Heidelberg (1988).
2. V. M. Kovenya and N. N. Yanenko, *Splitting Method in Gas-Dynamic Problems* [in Russian], Nauka, Novosibirsk (1981).
3. D. Anderson, J. Tannehill, and R. Pletcher, *Computational Fluid Mechanics and Heat Transfer*, Hemisphere, New York (1984).
4. D. S. Sheng, "Review of numerical methods for solving the Navier–Stokes equations for compressible gas flows," *Aerokosm. Tekh.*, **4**, No. 2, 65–92 (1986).
5. Yu. P. Golovachev, *Numerical Simulation of Viscous Gas Flows in the Shock Layer* [in Russian], Nauka, Moscow (1996).
6. A. I. Tolstykh, *Compact Difference Schemes and Their Application to Aerohydrodynamic Problems* [in Russian], Nauka, Moscow (1990).
7. A. N. Gil'manov, *Methods of Adaptive Grids in Gas-Dynamic Problems* [in Russian], Fizmatlit, Moscow (2000).
8. *Comput. Fluids*, **27**, Nos. 5/6, 551–740 (1998). [Spec. issue selected papers from the 6th Int. Symp. on Comput. Fluid Dynamics, Lake Tahoe (1995).]
9. *Comput. Fluids*, **33**, Nos. 5/6 (2004). (Spec. issue Appl. Math. for Industr. Probl.)
10. *Comput. Fluid Dynamics J.*, **13**, No. 2 (2004). [Spec. issue selected papers from 4th Asian Workshop on Computational Fluid Dynamics, Tokyo (2004)].
11. V. M. Kovenya and A. Yu. Slyunyaev, "Modifications of splitting algorithms for solving the Euler and Navier–Stokes equations," *Vychisl. Tekhnol.*, **12**, No. 3, 71–86 (2007).
12. V. M. Kovenya and A. Yu. Slyunyaev, "Modeling of supersonic gas flows in a duct," *Vychisl. Tekhnol.*, **12**, No. 4, 41–50 (2007).
13. He Yuanyuan, Le Jialing, Ni Hongli, "Numerical research of airframe/engine integrative hypersonic vehicle," in: *Proc. of the 12th Int. Conf. on the Methods of Aerophysical Research* (Novosibirsk, June 28–July 3, 2004), Part 2, Nonparel, Novosibirsk (2004), pp. 94–100.
14. L. G. Loitsyanskii, *Mechanics of Liquids and Gases*, Pergamon Press, Oxford-New York (1966).